Estimating Ice Shelf Thickness in Grounding Zones of the Filchner-Ronne Ice Shelf with Tidal Flexure from ICESat-2

Journal:	*Journal of Glaciology*
Manuscript ID	JOG-2026-0055
Manuscript Type:	Article
Date Submitted by the Author:	17-Apr-2026
Complete List of Authors:	Elgart, Faye; Massachusetts Institute of Technology, Earth, Atmospheric, and Planetary Sciences Minchew, Brent; Massachusetts Institute of Technology, Department of Earth, Atmospheric and Planetary Sciences
Keywords:	Antarctic glaciology, Ice shelves, Laser altimetry
Abstract:	In the grounding zones of Antarctic ice sheets, grounded ice sheets become floating ice shelves at the triple junction of the ice, ocean, and bedrock. Ice downstream of the grounding line rises and falls with ocean tides while ice upstream of it does not, creating kilometers wide flexure zones. Ice thickness in the flexure zone cannot be well estimated by assuming it is in hydrostatic equilibrium. Here we develop and apply an observationally-constrained inversion based on the tidal flexure of ice shelves, using repeat-track ICESat-2 altimetry data and an elastic beam bending model, to infer ice thickness and thickness gradient close to grounding lines. We apply this method to Institute Ice Stream, Foundation Ice Stream, and Recovery Glacier on the Filchner-Ronne Ice Shelf (FRIS) and find that flexure-derived ice thickness can be locally up to approximately 10% greater than the hydrostatically derived ice thickness from BedMachine. We also find that ice in these three grounding zones is relatively stiff, with a mean effective Young's modulus (E*) of 6.5 GPa. If ice in grounding zones around Antarctica is indeed thicker than commonly estimated, as found here, this may have far-reaching implications for ice sheet modeling.


SCHOLARONE
MANUSCRIPTS

Estimating Ice Shelf Thickness in Grounding Zones of the Filchner-Ronne Ice Shelf with Tidal Flexure from ICESat-2

Faye ELGART[1,2] and Brent MINCHEW[1,3]

[1]*Department of Earth, Atmospheric, and Planetary Sciences, Massachusetts Institute of Technology, Cambridge, MA, USA*

[2]*Laboratoire de Glaciologie, Université libre de Bruxelles (ULB), Brussels, Belgium*

[3]*Division of Geological and Planetary Sciences, California Institute of Technology, Pasadena, CA, USA*

Correspondence: Faye Elgart <faye.hendley.elgart@ulb.be>

ABSTRACT.

In the grounding zones of Antarctic ice sheets, grounded ice sheets become floating ice shelves at the triple junction of the ice, ocean, and bedrock. Ice downstream of the grounding line rises and falls with ocean tides while ice upstream of it does not, creating kilometers wide flexure zones. Ice thickness in the flexure zone cannot be well estimated by assuming it is in hydrostatic equilibrium. Here we develop and apply an observationally-constrained inversion based on the tidal flexure of ice shelves, using repeat-track ICESat-2 altimetry data and an elastic beam bending model, to infer ice thickness and thickness gradient close to grounding lines. We apply this method to Institute Ice Stream, Foundation Ice Stream, and Recovery Glacier on the Filchner-Ronne Ice Shelf (FRIS) and find that flexure-derived ice thickness can be locally up to approximately 10% greater than the hydrostatically derived ice thickness from BedMachine. We also find that ice in these three grounding zones is relatively stiff, with a mean effective Young's modulus (E^*) of 6.5 GPa. If ice in grounding zones around Antarctica is indeed thicker than commonly estimated, as found here, this may have far-reaching implications for ice sheet modeling.

INTRODUCTION

Continent-wide ice thickness maps are a fundamental input to catchment-scale and larger models of Antarctica that model the current state and future evolution of the Antarctic Ice Sheet (AIS). One of the largest data assimilation undertakings in glaciology seeks to elucidate the topography of the bed underneath the AIS (Frémand, A. C. and 83 others, 2023; Morlighem M and 36 others, 2020), and, since the ice surface elevation is observable (Howat and others, 2019), necessarily determine the ice thickness as well.

Ice-penetrating radar thickness measurements are sparse and may always be sparse because there are no space-borne ice-penetrating radar instruments due to frequency band restrictions (some exist on Mars (Seu and others, 2007; Jordan and others, 2009)). Direct ice thickness inferences must be made with airborne or ground-based instruments. The first full Antarctic ice sheet models used interpolated maps of ice thickness from the first of these measurements, with roughly 100 km resolution (e.g., Budd and Smith (1982); Oerlemans (1982)) which improved as new measurement campaigns were completed (Huybrechts and others, 2000; Warner and Budd, 2000), but left gaps in undersampled or unsampled regions.

As detailed maps of Antarctic ice surface velocity became available in the satellite era, it became possible to combine the sparse measurements of ice thickness with the ice surface velocity to infer a pan-Antarctic ice thickness that conserved mass and minimized the misfit between the modeled and observed ice thicknesses (Morlighem and others, 2011). This project became BedMachine, which assimilates the field's airborne ice-penetrating radar thickness record with remotely sensed high-resolution ice velocity maps, as well as gravimetry and seismic measurements, and using streamline diffusion methods where ice is slow-moving and can be less well approximated by mass conservation. The project brings together dozens of institutions and the work of hundreds of researchers to produce a map of the sub-ice sheet bathymetry of Antarctica and of Greenland (Morlighem and others, 2014, 2017; Morlighem M and 36 others, 2020).

On ice shelves, a different approach is taken because the thickness of a free-floating ice shelf can be inferred by its height of flotation above the sea surface, e.g., Griggs and Bamber (2009); Le Brocq and others (2010); Smith B and 14 others (2020); Adusumilli and others (2020), with a correction for firn densification (Chartrand and Howat, 2023). In BedMachine, the assumption of hydrostatic equilibrium is applied downstream of the grounding line, with a spatially varying firn correction calibrated against available radar-derived ice shelf thickness data. However, near the grounding line, the hydrostatic assumption breaks down, as the ice shelf is mechanically coupled to the upstream ice sheet and flexes, rather than

floats, on top of ocean tides that cycle around Antarctica every 12-24 hours (Padman and others, 2018).

BedMachine imposes a smooth transition between grounded and ungrounded ice over the first few kilometers of downstream ice, which can require changes in ice thickness of more than one kilometer (Morlighem M and 36 others, 2020). While the reported uncertainty in ice thickness in areas with dense radar sounding is 36 m, the authors note that in areas where sub-ice shelf bathymetry measurements are sparse, uncertainty may exceed 500 m (Morlighem, 2022), because modeling sub-ice shelf cavity circulation and resonance of tides within the cavity requires detailed knowledge about the sub-ice shelf bathymetry, and a modeled tidal height must be subtracted from the observed ice shelf height to compute the ice thickness hydrostatically (Adusumilli and others, 2018). This is especially true close to the grounding line, where incorporating tidal flexure observations into tidal models is an active area of research (Begeman and others, 2020).

The hydrostatic-flotation approach systematically underestimates ice thickness in the flexure zone because part of the ice weight is not borne by buoyancy. Upstream bending stresses transmitted from grounded ice, intermittent basal contact, and compressive buttressing all supply additional vertical support, depressing the ice surface relative to a freely floating slab.

Here, we exploit the tidal flexure of ice shelves in the grounding zone to develop an observationally-constrained inversion for ice thickness and thickness gradient in the grounding zone. We use differenced repeat track observations of the ice surface height from ICESat-2 to observe vertical tidal deflection, and model this deflection with an elastic beam model of varying thickness. We apply the method to three basins of the Filchner-Ronne Ice Shelf (FRIS) with a diverse set of geometries and settings: Institute Ice Stream (IIS), Foundation Ice Stream (FIS), and Recovery Glacier (RG) (Fig. 1). We find that an ensemble of parameterized ice thicknesses constrained by the observations suggests that ice near the landward limit of tidal flexure may be locally on the order of ten percent thicker than estimated by hydrostatic methods. This has implications for catchment-scale modeling of the evolution of the AIS, particularly as ice thickness in the grounding zone is fundamental to calculating basal melt rate in the grounding zone, which is one of the single most important and least-well constrained parameters controlling the onset of rapid grounding line retreat and future sea level rise (Pattyn, 2017; Seroussi H and 46 others, 2020; Hill and others, 2021).

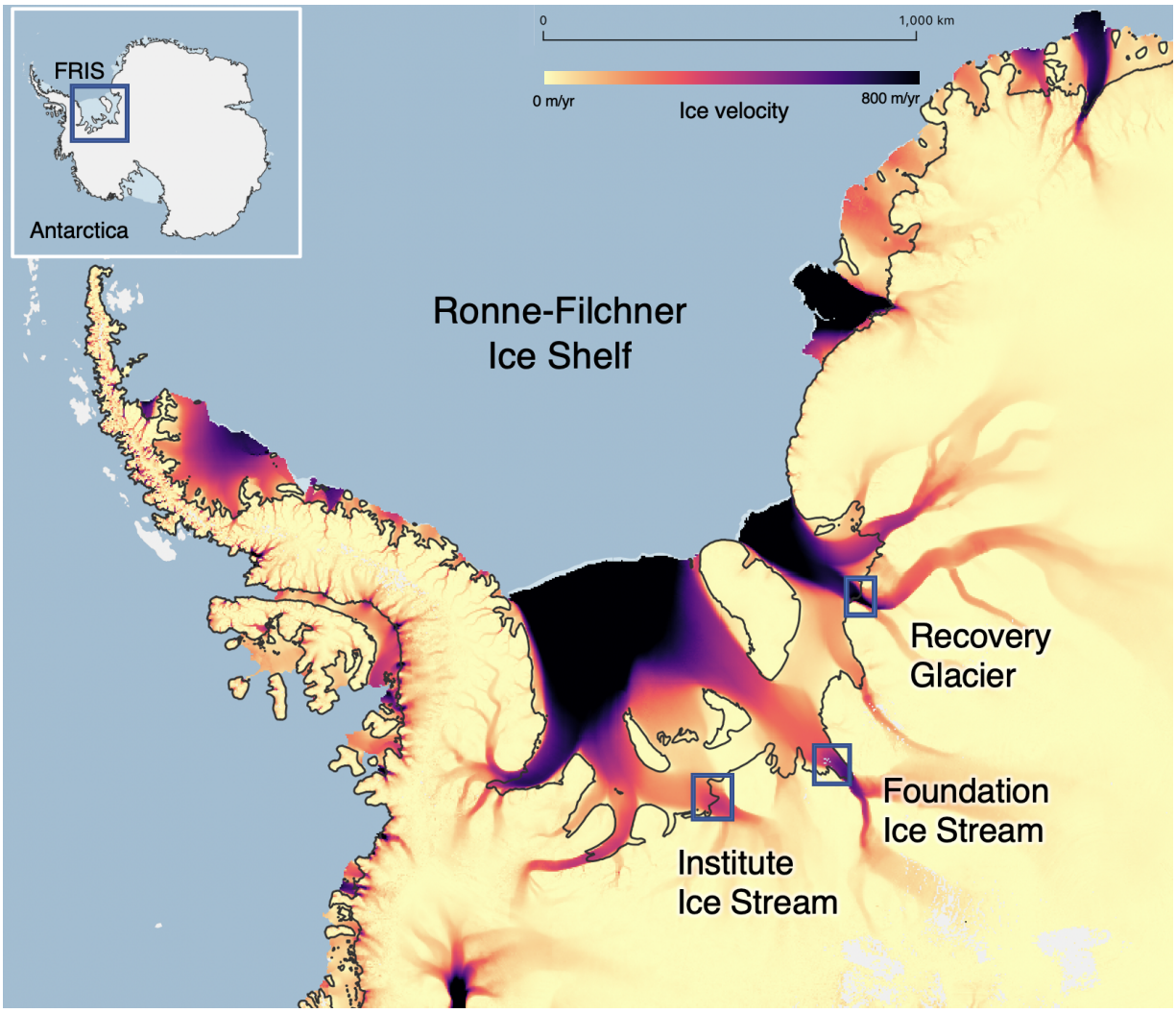

Fig. 1. Major basins of the Filchner-Ronne Ice Shelf and its situation on Antarctica, inset. We present new inferences of ice thickness in the grounding zones of Institute Ice Stream, Foundation Ice Stream, and Recovery Glacier.

METHODS

We infer ice thickness in three grounding zones on FRIS (Fig. 1), chosen for having ICESat-2 ground tracks that cross the grounding line roughly perpendicularly to the direction of ice flow and being at least approximately one flexural wavelength (15 km) away from confining topography. We use repeat track satellite altimetry observations of tidal flexure and solve a forward model of ice shelf flexure many times to minimize the misfit between modeled ice surface deflection and the vertical flexure observations while varying the ice thickness gradient and effective Young's modulus in the flexure zone. Here we describe our forward model, the parameter space for our inverse approach, and our observational method.

Forward Model of Tidal Flexure

Ice near the grounding line that flexes on top of ocean tides can be modeled as an elastic beam of varying thickness (Vaughan, 1995; Sayag and Worster, 2011, 2013; Marsh and others, 2014; Rosier and others, 2017). If the ice thickness $h(x)$ of the flexing portion of ice and Young's modulus E are both known, the vertical deflection w of the beam can be computed numerically from the Euler-Bernoulli beam bending equation, after Holdsworth (1969) and Robin (1958):

$$\frac{d^2}{dx^2}\Big[D(x)\frac{d^2w}{dx^2}\Big] = \rho_w g\big[A_0 - w(x)\big], \tag{1}$$

where A_0 is the far-field sea level, ρ_w is the mass density of seawater, g is gravitational acceleration, and D is the spatially variable flexural rigidity of the beam:

$$D(x) = \frac{Eh^3}{12(1-\nu^2)} \tag{2}$$

where ν is the Poisson's ratio of ice, here taken to be 0.3 (Schulson and Duval, 2011). The forward problem finds the deflection w given full information about $D(x)$, and can be readily solved numerically by central differences as described in Elgart and others (2026) and summarized in Supplementary Material S1.

In Elgart and others (2026), we use this problem setup in three grounding zones on the Ross Ice Shelf, arguing that when the local ice thickness is well known, what can be inferred from (1) is the *effective* Young's modulus E^* only, a bulk parameter that encodes information about the local elastic properties of the ice-ocean-bedrock system near the grounding line (Fig. 2). We found significant spatial variation in E^*, with a mean of 4.7 $\pm$ 2.4 GPa on the Ross Ice Shelf, reflecting that varying and intersecting

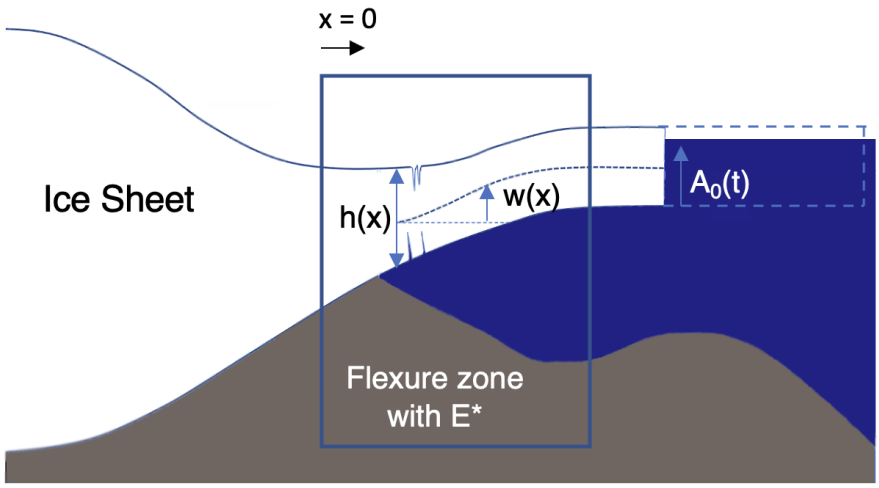

Fig. 2. Sketch of the problem setup. We seek to infer ice thickness $h(x)$ from observations of the vertical tidal deflection $w(x)$ from ICESat-2. The flexure zone has an effective Young's modulus E^* reflecting the combined effects of all physical processes that might affect the observable flexure.

physical processes in the flexure zone may affect the ice's observable surface flexure, and building on the methodology of Vaughan (1995) to accommodate a spatially variable $h(x)$.

This is in contrast to textbook values for the Young's modulus of ice, commonly referenced at 9 GPa (Hooke, 2005), and to other flexure-inferred values of Young's modulus which can be up to an order of magnitude smaller (e.g., Vaughan (1995)). To accommodate the order of magnitude variation within the literature, we vary E^* in the inverse problem from 1-9 GPa, as described below. We solve the forward problem for $w(x)$ many millions of times to jointly invert for the combinations of $h(x)$ and E^* that minimize the misfit between modeled and observed tidal flexure.

Inverse Problem for Ice Thickness

The inverse problem seeks to infer properties of the beam given its observed flexure. This inverse problem is mathematically ill-posed, meaning that solving directly for $h(x)$ is unfeasible because solutions may oscillate about the correct one and the problem is very sensitive to noise and to its boundary conditions (Lucchinetti and Stüssi, 2002). Therefore, to find the most likely ice thickness gradient near the grounding line, we solve the forward problem many times with a range of parameterized ice thickness gradients, values for effective Young's modulus E^*, and boundary locations.

We seek to minimize the misfit between modeled and observed flexure within the solution space of these parameters. Since ice thickness and E^* are coupled as in (2), we expect many combinations of $h(x)$ and

E^* to produce similar deflection curves. Below, we describe the parameter ranges we select to manage the ill-posedness of the problem and explore the solution space of best fitting ice stiffnesses.

We parameterize the thickness profile $h(x)$ as a cubic Hermite spline defined by four parameters: the thickness values h and slopes $\partial h/\partial x$ at both the landward and seaward ends of the flexure zone (see Supplementary Material S1). This allows us to characterize a range of physically plausible thickness gradients with relatively few parameters.

We vary the landward end member thickness between $\pm$ 250 m of the maximum BedMachine thickness along the flexure zone. This allows the high end of reported estimated uncertainty in Morlighem (2022) to be investigated. We vary seaward end member thickness by $\pm$ 100 m of the minimum BedMachine thickness along the flexure zone. We use a smaller range at the seaward edge of the problem domain because we expect the hydrostatic assumption to better approximate the ice shelf thickness away from the grounding line. The value of 100 m is as reported for ice shelf thickness uncertainty in BedMachine, and largely originates in uncertainty in tidal amplitude, which must be subtracted from the observed freeboard ice shelf height, and in turn originates in uncertainty in sub-ice-shelf cavity bathymetry (Padman and others, 2018).

The slope at the landward boundary, $\partial h/\partial x$, is varied between -0.05 and 0.005, a physically plausible range of end member thickness slopes that allow for a variety of thickness gradients. We expect a generally decreasing thickness profile as we move seaward, but wish to allow for a range of scenarios capturing local variation in thickness gradient. The slope at the seaward boundary is varied between -0.005 and 0. Here we expect very small to zero slope in thickness, assuming the ice has transitioned to a fully extensional regime at the seaward extent of the flexure zone, where an increasing slope in thickness would be unphysical. Ten linearly spaced points between these ranges are used for each parameter, resulting in 10^4 potential solutions $h(x)$. This choice of polynomial parameterization of ice thickness results in a resolution of about half the length of the flexure zone, with a reasonably small number of parameters to vary, and we generally expect no finer resolution in thickness to be supportable by the observable data.

For the effective Young's modulus E^*, we test a range of values for E^* between 1 GPa and 9 GPa in increments of 1 GPa. This covers the lower end of physically plausible elastic moduli, in the range found by Vaughan (1995) and used by some elastic ice bending models (Marsh and others, 2014), middle values, as found in Elgart and others (2026) and used by several other ice bending models (Rosier and others, 2017), and includes the common laboratory value for E of 9 GPa.

The inverse problem is also sensitive to the position of the landward boundary, which is analogous to the broadly observed model sensitivity to grounding line position, though as before we note that we do not assume that the grounding line position is identical to the landward extent of tidal flexure. To address this, we first estimate the approximate landward extent of tidal flexure, x_{gl}, then allow the problem domain to extend to points 500 m landward or seaward of the initial estimated position. This allows for small errors in surface slope induced by interpolation or differencing of repeat tracks to not dominate the resultant inference, and is on the order of or less than grounding line position resolution in Antarctic models (Pattyn and others, 2013). The result of the inversion was not similarly sensitive to the precise location of the seaward boundary.

Tidal Flexure from ICESat-2

Observing tidal flexure near the grounding line requires repeat track observations of the ice surface height in the flexure zone at different points in the tidal cycle (Fricker and Padman, 2006). Here, we use differenced repeat tracks of ATL06 ice surface height data at Institute Ice Stream, Recovery Glacier, and Foundation Ice Stream, on FRIS.

Since we are interested in the long-wavelength, low frequency tidal signal, and ATL06 data are noisy, we smooth and filter the data several times before and after differencing the mean ice height from each individual track. These data are processed identically as Elgart and others (2026). This yields the height anomaly per track, and we interpret this directly as $w(x)$, as given enough tracks, the mean ice height will approximate the unstressed ($A_0 = 0$) ice shelf position. After removing tracks with any discontinuities or clear signs of residual noise due to clouds or other effects, and tracks with amplitude too close to the unstressed state to produce a meaningful inversion, we obtain six flexure profiles at Institute, using beam pair 1 (**gt1r** and **gt1l**) from ICESat-2 Reference Ground Track (RGT) 1367, nine at Foundation, using **gt3r** and **gt3l** from RGT 1351, and six profiles at Recovery, using **gt3r** and **gt3l** from RGT 612 (see Fig. 3).

We manually select the approximate location of the landward extent of tidal flexure and allow it to vary within 500 m of this position as described above. Similarly, we identify the constant value of the ice surface height at the seaward edge of the flexure zone from the flexure data at each track and define A_0 as the height difference between these two points. Because this effectively zeros the seaward edge of the problem domain, no dynamic atmospheric correction is needed. The inversion is not highly sensitive to

the position of the seaward edge provided that it is far enough away from the clearly flexing portion of the observed data. This results in roughly 150 data points describing the flexure curve $w(x)$ for each track after interpolation.

The surface mass balance (SMB) on FRIS, mainly consisting of snow accumulation, is on the order of 0.2 to 2 meters per year (Mottram and others, 2021; Van Wessem JM and 18 others, 2018). SMB maps on Antarctica are broadly available at 25 km resolution, and at 5 km only in some areas. Since this could only be applied as a constant valued offset at the resolution of our data, and the measurement timescale is very short, and we difference the mean ice height from each individual track, we apply no further correction for snow.

Acceptance Criteria

Because of the coupled relationship between ice thickness and effective Young's modulus, the small differences between adjacent thickness solutions, noise in the data, and the tendency of the best linear elastic beam bending solutions to fit nearly arbitrarily well to observed data (Rosier and others, 2017), we wish to explore the solution space of the problem rather than pick the single best solution.

We define an acceptance criterion for $h(x)$ such that for a given track, at all points (E^*, x_{gl}), an ice thickness $h(x)$ is acceptably good when the resultant RMS misfit between a modeled beam with that $h(x)$ and the observed flexure is either: within 0.1 m of the minimum RMS of the best fitting solution at that track, RMS_{min}, or, less than 2*RMS_{min}, whichever is smaller. The threshold of 0.1 m RMS misfit was chosen because we expect model error to dominate measurement error: ICESat-2 ATL06 data is accurate to better than 3 cm with better than 9 cm of surface measurement precision (Brunt and others, 2019), and observed tracks consist of between 100 and 200 (related) measurement points. The misfit threshold chosen here reflects that several centimeters of misfit over tens of kilometers of flexure corresponds to very small deviations in slope: the vertical scale in Fig. 2 and Fig. 3 is greatly exaggerated.

From all the accepted $h(x)$ at each site, we calculate a median inferred $h(x)$, as well as the 25th and 75th percentile $h(x)$, and the $h(x)$ of the spatially averaged best fitting solutions $h(x)$; that is, the top 1% of solutions by RMS. Contours of the RMS misfit space and number of accepted $h(x)$ for each track are available in Supplementary Material S1.

RESULTS

We jointly invert for ice thickness gradient and effective Young's modulus near the grounding line in three basins on FRIS, and find that all three sites show substantial differences in thickness gradient compared to the BedMachine solutions (Fig. 4). The flexure-inferred thicknesses are locally on the order of 10-15% thicker than the interpolated hydrostatic thickness from BedMachine in the flexure zone near the grounding line, while they broadly converge around the hydrostatic thickness at the seaward edge of the flexure zone. This corresponds to differences of up to several hundred meters at some locations, or up to about 20% of the local ice thickness.

After testing 10^4 potential solutions $h(x)$ at all possible combinations of E^* and grounding line position as described above, we admit between 10^4 and 10^6 solutions $h(x)$ at each site from all tracks combined. Fig. 4 shows the median ice thickness at each point in space of all acceptably good (see above) solutions $h(x)$ as a thick blue line. The 25th to 75th percentile of accepted $h(x)$ in space are shown shaded, in blue. We also plot the mean $h(x)$ of the best approximately 1% of accepted solutions by RMS as a dashed line. This gives a sense of the density of the solution space; e.g., where the best solutions within the acceptably good solutions tend to fall relative to the median. The BedMachine thickness and its estimated uncertainty are shown in black. Also shown are a random sample of the set of 10^4 potential solutions $h(x)$ that are tested at each potential effective Young's modulus and grounding line position, illustrating the full range of all tested $h(x)$.

Fig. 5 illustrates where in the grid searched (E^*, x_{gl}) the accepted solutions originate. All sites show a tendency towards higher effective Young's moduli within the tested range, shown by darker shading indicating lower minimum misfit at each point in the grid search relative to the global minimum at that site (Fig. 5, left). The mean effective Young's modulus E^* across all three sites is 6.5 GPa. The mean E^* of all accepted solutions at Institute Ice Stream is 7.5 GPa. At Foundation Ice Stream, it is 6.8 GPa, and at Recovery Glacier it is 6.1 GPa.

The right side of Fig. 5 illustrates how many solutions fit similarly well enough to the global minimum to be included as accepted solutions. At Institute Ice Stream, which has deeper and smaller valleys in its misfit space than the other sites, many (thousands) fewer solutions were accepted than at the other sites. Very few solutions with Young's moduli below 4 GPa were accepted at any site. In Fig. 5, a tendency towards solutions that gather at the upper right corner of the grid search can be observed. While ideally

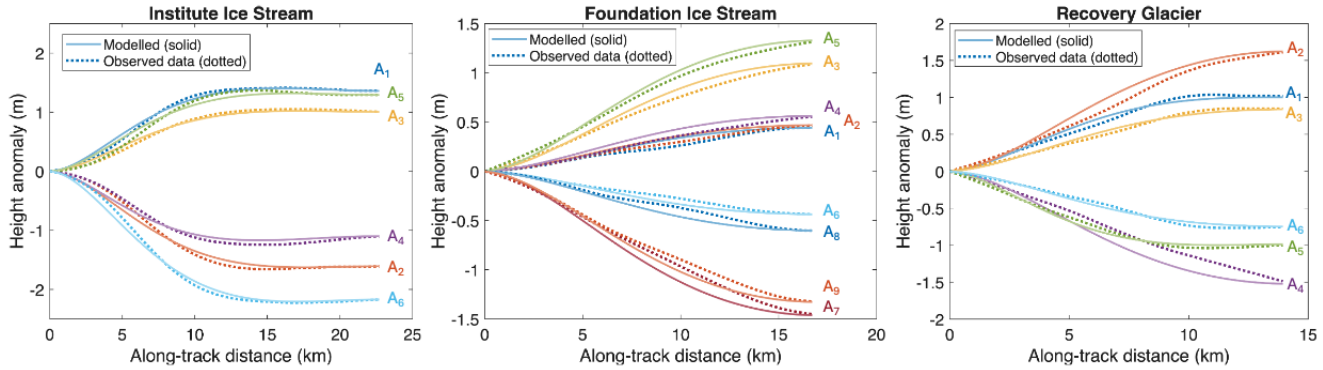

Fig. 3. Modeled and observed vertical tidal flexure at Institute Ice Stream, Foundation Ice Stream, and Recovery Glacier. Each pair of modeled (solid) and observed (dashed) lines occurs at a different point in time and in the tidal cycle, with tidal amplitude A_i. We note that the A_i are not the same between sites. The modeled flexure here depicts the single best fitting pair of E^* and $h(x)$ for that track. We accept solutions with up to twice (or a fixed value, whichever is less) the misfit at each track as seen here; see Acceptance Criteria subsection.

the results of an ill-posed inverse problem fall within a well defined region away from the edges of the search space, in practice this is not always possible. Here, since we admit solutions from a broad section of the search space, because there is no clear physical argument for E^* much higher than 9 GPa, and for reasons discussed further in Supplementary Material S1, we find this to be an acceptable compromise. The misfit space at Institute Ice Stream is also more densely featured than the other two sites.

Fig. 3 shows the vertical tidal flexure data at each site, processed as described above, paired with the best fitting modeled solution at each labeled track. Between six and nine tracks are found to be suitable for modeling at each site.

DISCUSSION

Ice thickness near the grounding line is one of the most important and least well known parameters in Antarctic ice sheet modeling because continent-wide fundamental community data products rely on the hydrostatic assumption for ice shelf thickness, and the hydrostatic assumption breaks down at the grounding line. Direct ice-penetrating radar thickness measurements close to the grounding line are sparse and require dedicated measurement campaigns. BedMachine assimilates these data where they exist, and new versions continue to incorporate new data, but interpreting radargrams near the grounding line is notoriously difficult (MacGregor and others, 2011), and in regions where radar data are sparse, the hydrostatic assumption will always underlie ice thickness in the grounding zone.

Tidal flexure offers a complementary constraint on ice thickness in the grounding zone that is physically

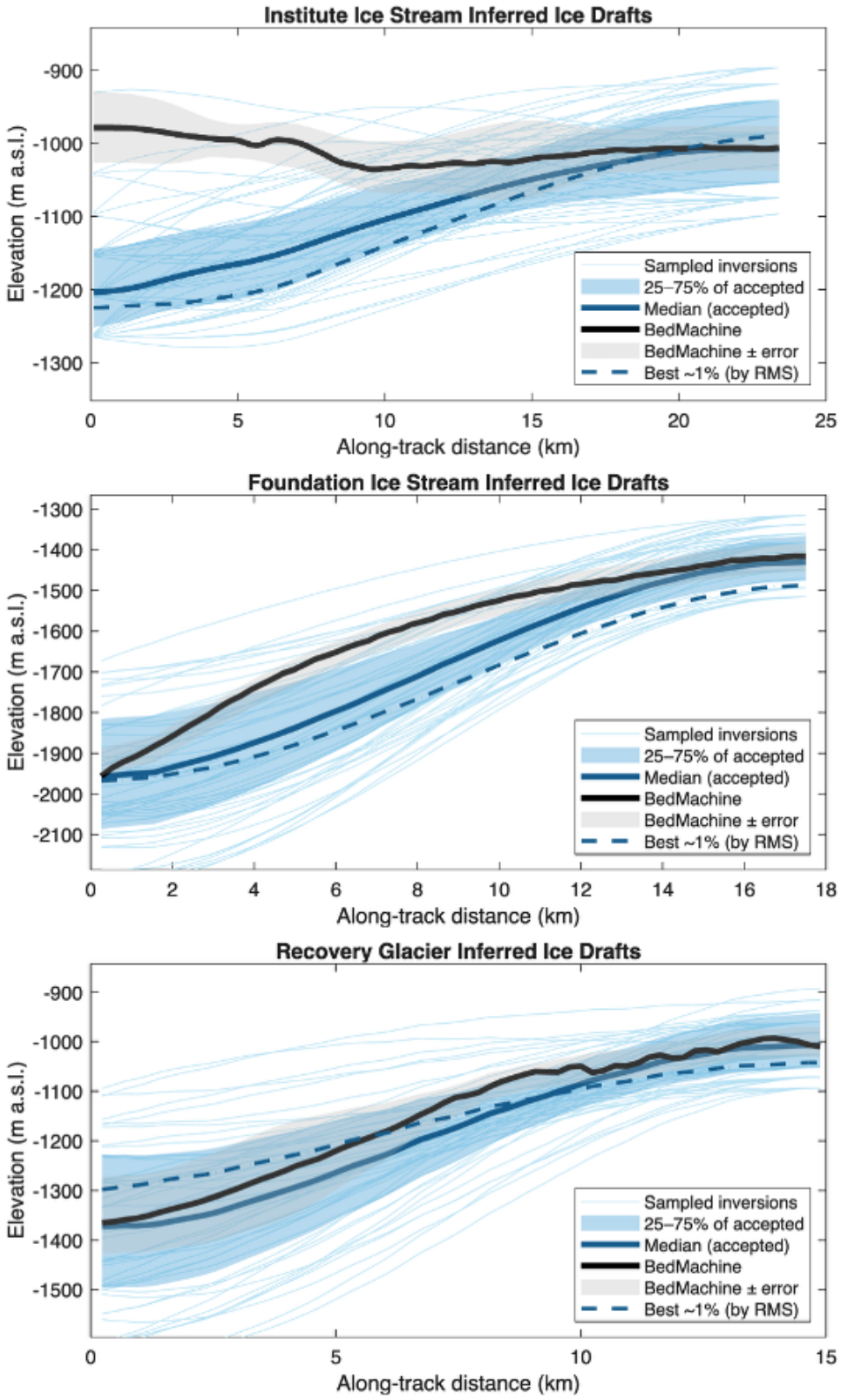

Fig. 4. Inferred ice drafts at the three study sites, using ice surface height from REMA, the Reference Elevation Map of Antarctica (Howat and others, 2019). Light blue lines sample the solution space of all potential $h(x)$. The blue envelope and blue lines depict the density of the solution space of accepted $h(x)$. The BedMachine thickness and associated uncertainty are shown in black.

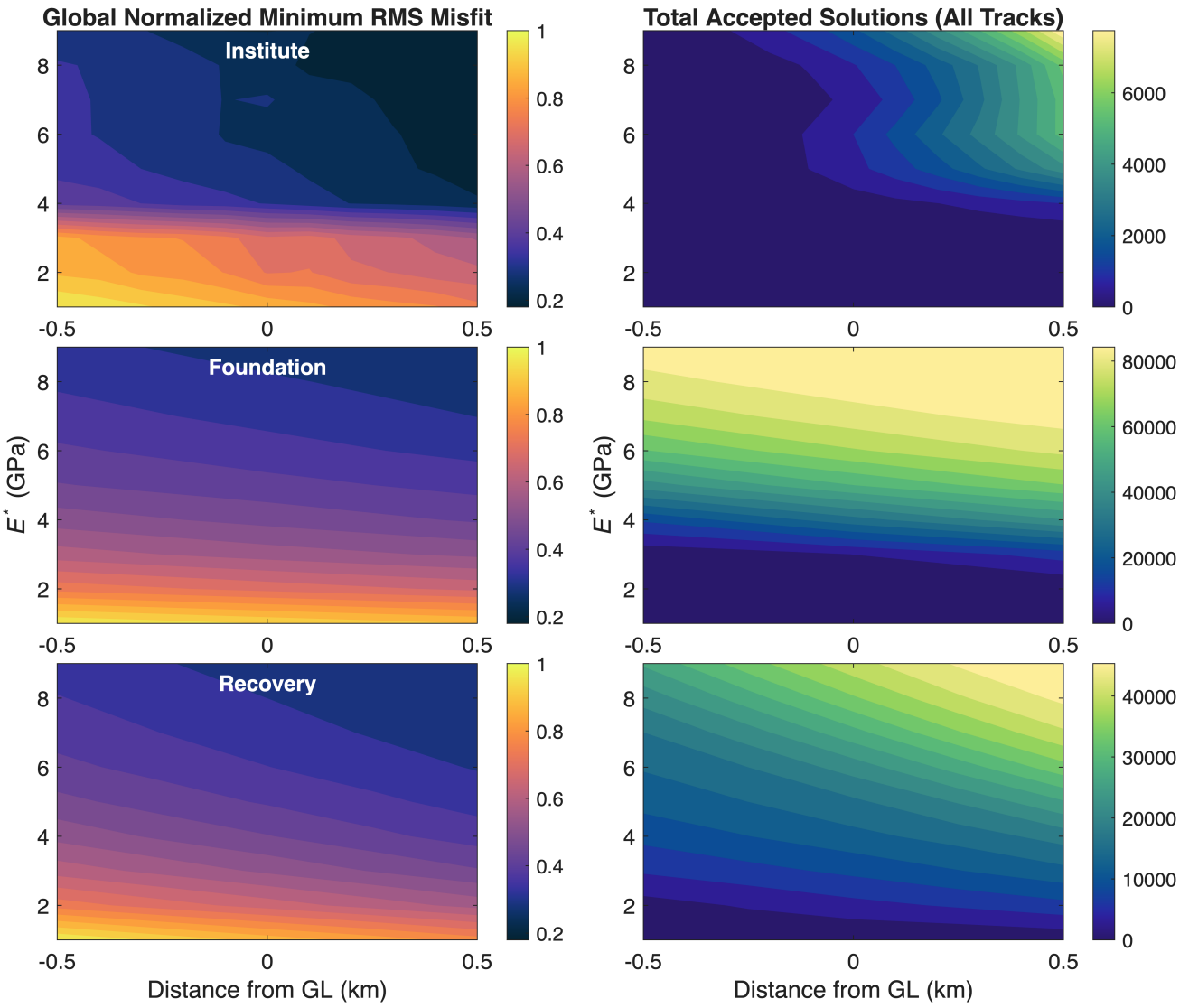

Fig. 5. The normalized misfit and total accepted solutions across all tracks, at all sites. The darkest regions on the left hand column indicate regions where well-fitting solutions are found. The right hand column indicates how many such solutions are found at all points (E^*, x_{gl}).

motivated in this dynamically critical region. By making a different set of assumptions, namely, that ice is linear elastic on tidal timescales; that longitudinal stresses are significantly greater than across-flow stresses such that a one-dimensional beam bending approach can be followed, as opposed to a more complex plate-bending formulation; and that the intersecting physical properties of the ice-ocean-bed system near the grounding line can be adequately parameterized by a bulk effective Young's modulus, we find that the hydrostatic assumption underestimates the ice thickness in the flexure zone, especially near the grounding line. The three study sites all have flexure-inferred thickness gradients that are locally up to approximately 200 meters thicker than the hydrostatically-inferred BedMachine solutions.

The effective Young's modulus and ice thickness are coupled in the beam-bending equation as equation 2. With flexure held constant, a ten percent increase in h would require a 25 percent decrease in E^*. This is the origin of much of the degeneracy in the contour plots in Supplementary Material S1. However, here, both higher h and higher E^* give better fits. This indicates that the values of both parameters are physically meaningful, as opposed to representing a simple tradeoff between the two. By allowing $h(x)$ and E^* to vary within physically plausible ranges and defining a relatively broad acceptability criterion, we take an ensemble approach that admits many plausible ice thickness profiles at each site. Together, they recover the anticipated tendency of the hydrostatic assumption to underestimate ice thickness at the landward edge of the flexure zone. The expected sign is recovered in all three cases: the hydrostatic assumption underestimates ice thickness near the grounding line because the ice shelf is mechanically coupled to the upstream grounded ice and therefore part of its weight is not borne by buoyancy.

Institute Ice Stream is cold, and relatively quiescent, with little grounding line motion. The basin is wide, the flexure profiles are well-behaved, and radar transects are not especially dense or sparse (Janout and others, 2021; Morlighem M and 36 others, 2020; Adusumilli and others, 2020; Mueller and others, 2018). Foundation Ice Stream and Recovery Glacier are smaller, narrower, faster, and deeper, and together, they represent a range of geometric, glaciological, and oceanographic settings, on one of Antarctica's largest cold-water glaciers. Thus, ice thickness in the grounding zone may likely be similarly underestimated in many similar basins of FRIS and other ice shelves.

No prior information about the effective Young's modulus at the test sites is required in order to infer a most likely envelope of ice thicknesses based on tidal flexure. However, some emerges anyway from the inversion: we find that these are likely particularly stiff flexure zones, with a mean E^* of 6.5 GPa across the sites. This is in contrast to the results of Elgart and others (2026) on the Ross Ice Shelf, where we find

an average E^* of 4.7 ± 2.4 GPa in a zone of dense ice-penetrating radar measurements, and to other, lower flexure-inferred values of E^* in the literature. While a high effective Young's modulus makes physical sense in the context of FRIS and closely resembles the idealized problem setup in Fig. 2, where the landward extent of the flexure zone is nearly the same as the grounding line position and shifts very little between tracks, and the ice is cold, thick, and intact, this implies the flexure zone in other places on the AIS may be significantly more flexible or softer than found on FRIS. There is increasing evidence that the bed of the AIS is fundamentally mixed, with hard and soft, and frozen and deformable regions (Kazmierczak and others, 2024), which may contribute to the spatial variability in inferred E^* and potentially quantify or help parameterize the character of the bed in ice sheet models.

Ice thickness at the grounding line is a fundamental glaciological variable that touches many problems in the field. It directly enters continental mass balance calculations (Smith B and 14 others, 2020). Basal melt rate at the grounding line is one of the single greatest sources of uncertainty in projections of the future sea level rise, and is often calculated by continuity of mass (Adusumilli and others, 2020), which requires ice thickness at the grounding line. This in turn links glaciological and ocean and earth system models, by affecting inputs to cavity geometry and circulation models. Ice thickness at the grounding line influences calculations of grounding line flux and stress balance, forming the fundamental statement of the Marine Ice Sheet Instability (Schoof, 2007). Finally, the initialization and calibration of continental ice sheet models relies on a full map of Antarctic ice thickness that is as accurate as possible. If ice thickness is systematically underestimated at the grounding line, this may have far-reaching implications for uncertainty in models of the rate and amount of committed future sea level rise from Antarctica.

CONCLUSION

Ice thickness near the grounding line is a strong control on ice sheet-shelf dynamics (Schoof, 2007), and here we find that ice thickness in grounding zones around Antarctica, especially in radar-poor regions, may be significantly and systematically underestimated because the hydrostatic approximation does not hold well in the grounding zone. Direct measurements of ice thickness in grounding zones are sparse and may always be sparse because there are no satellite-borne ice-penetrating radar instruments, but any in situ measurements of the fundamental properties of ice in grounding zones will always help move toward a model of Antarctica that meaningfully and closely resembles the observational record. If ice thickness in the grounding zone is indeed currently underestimated in many basins around Antarctica, a careful,

regionally heterogeneous and observationally constrained correction may aid in reducing the spread in modeled uncertainty in projections of future sea level rise in the coming decades and centuries.

COMPETING INTERESTS

BM is a co-founder of Arête Glacier Initiative (areteglaciers.org), where he maintains affiliation through his allowance for outside professional activities provided by his university. Arête is a non-profit organization (currently a fiscally sponsored organization of the 401(c) 3 Digital Harbor Foundation) founded in 2024 to provide funding to glaciological research focused on sea-level rise. BM and FE declare no financial, personal, nor professional conflicts of interest.

ACKNOWLEDGMENTS

The authors would like to thank Colin Meyer for contributions to the method that made this paper possible, Kasia Warburton for contributions to early discussions, Ben Smith, Camilla Cattania, and John Marshall for providing helpful feedback. FE received funding through NASA FINESST award 80NSSC21K1619, and the John W. Jarve (1978) Seed Fund at MIT, and the NEC Corporation Fund for Research in Computers and Communications at MIT. BM received funding through NSF-NERC award 1853918, the John W. Jarve (1978) Seed Fund at MIT, and the NEC Corporation Fund for Research in Computers and Communications at MIT.

REFERENCES

Adusumilli S, Fricker HA, Siegfried MR, Padman L, Paolo FS and Ligtenberg SRM (2018) Variable basal melt rates of Antarctic Peninsula Ice Shelves, 1994–2016. *Geophysical Research Letters*, **45**(9), 4086–4095 (doi: https://doi.org/10.1002/2017GL076652)

Adusumilli S, Fricker HA, Medley B, Padman L and Siegfried MR (2020) Interannual variations in meltwater input to the Southern Ocean from Antarctic ice shelves. *Nature Geoscience*, **13**, 616–620 (doi: 10.1038/s41561-020-0616-z)

Begeman CB, Tulaczyk S, Padman L, King M, Siegfried MR, Hodson TO and Fricker HA (2020) Tidal pressurization of the ocean cavity near an Antarctic Ice Shelf grounding line. *Journal of Geophysical Research: Oceans*, **125**(4), e2019JC015562 (doi: https://doi.org/10.1029/2019JC015562), e2019JC015562 10.1029/2019JC015562

Brunt KM, Neumann TA and Smith BE (2019) Assessment of ICESat-2 ice sheet surface heights, based on comparisons over the interior of the Antarctic Ice Sheet. *Geophysical Research Letters*, **46**(22), 13072–13078 (doi: https://doi.org/10.1029/2019GL084886)

Budd W and Smith I (1982) Large-scale numerical modelling of the Antarctic Ice Sheet. *Annals of Glaciology*, **3**, 42–49 (doi: 10.3189/S0260305500002500)

Chartrand AM and Howat IM (2023) A comparison of contemporaneous airborne altimetry and ice-thickness measurements of Antarctic ice shelves. *Journal of Glaciology*, **69**(278), 1663–1676 (doi: 10.1017/jog.2023.49)

Elgart F, Minchew B and Meyer CR (2026) Estimating effective elasticity in grounding zones of the Ross Ice Shelf with tidal flexure from ICESat-2. *Journal of Glaciology*, **72**, e23 (doi: 10.1017/jog.2026.10137)

Fricker HA and Padman L (2006) Ice shelf grounding zone structure from ICESat laser altimetry. *Geophysical Research Letters*, **33**(15) (doi: 10.1029/2006GL026907)

Frémand, A C and 83 others (2023) Antarctic Bedmap data: Findable, Accessible, Interoperable, and Reusable (FAIR) sharing of 60 years of ice bed, surface, and thickness data. *Earth System Science Data*, **15**(7), 2695–2710 (doi: 10.5194/essd-15-2695-2023)

Griggs JA and Bamber JL (2009) Ice shelf thickness over Larsen C, Antarctica, derived from satellite altimetry. *Geophysical Research Letters*, **36**(19) (doi: https://doi.org/10.1029/2009GL039527)

Hill EA, Rosier SH, Gudmundsson GH and Collins M (2021) Quantifying the potential future contribution to global mean sea level from the Filchner-Ronne basin, Antarctica. *Cryosphere*, **15**, 4675–4702 (doi: 10.5194/tc-15-4675-2021)

Holdsworth G (1969) Flexure of a floating ice tongue. *Journal of Glaciology*, **8**(54), 385–397 (doi: 10.3189/s0022143000026976)

Hooke RL (2005) *Principles of Glacier Mechanics*. Cambridge University Press, 2 edition

Howat IM, Porter C, Smith BE, Noh MJ and Morin P (2019) The Reference Elevation Model of Antarctica. *The Cryosphere*, **13**(2), 665–674 (doi: 10.5194/tc-13-665-2019)

Huybrechts P, Steinhage D, Wilhelms F and Bamber J (2000) Balance velocities and measured properties of the antarctic ice sheet from a new compilation of gridded data for modelling. *Annals of Glaciology*, **30**, 52–60 (doi: 10.3189/172756400781820778)

Janout MA, Hellmer HH, Hattermann T, Huhn O, Sültenfuss J, Østerhus S, Stulic L, Ryan S, Schröder M and Kanzow T (2021) FRIS revisited in 2018: On the circulation and water masses at the Filchner and Ronne Ice

Shelves in the southern Weddell Sea. *Journal of Geophysical Research: Oceans*, **126**(6), e2021JC017269 (doi: https://doi.org/10.1029/2021JC017269), e2021JC017269 2021JC017269

Jordan R, Picardi G, Plaut J, Wheeler K, Kirchner D, Safaeinili A, Johnson W, Seu R, Calabrese D, Zampolini E, Cicchetti A, Huff R, Gurnett D, Ivanov A, Kofman W, Orosei R, Thompson T, Edenhofer P and Bombaci O (2009) The Mars express MARSIS sounder instrument. *Planetary and Space Science*, **57**(14), 1975–1986, ISSN 0032-0633 (doi: https://doi.org/10.1016/j.pss.2009.09.016)

Kazmierczak E, Gregov T, Coulon V and Pattyn F (2024) A fast and simplified subglacial hydrological model for the Antarctic Ice Sheet and outlet glaciers. *The Cryosphere*, **18**(12), 5887–5911 (doi: 10.5194/tc-18-5887-2024)

Le Brocq AM, Payne AJ and Vieli A (2010) An improved Antarctic dataset for high resolution numerical ice sheet models (ALBMAP v1). *Earth System Science Data*, **2**(2), 247–260 (doi: 10.5194/essd-2-247-2010)

Lucchinetti E and Stüssi E (2002) Measuring the flexural rigidity in non-uniform beams using an inverse problem approach. *Inverse Problems*, **18**(3), 837 (doi: 10.1088/0266-5611/18/3/320)

MacGregor JA, Anandakrishnan S, Catania GA and Winebrenner DP (2011) The grounding zone of the Ross Ice Shelf, West Antarctica, from ice-penetrating radar. *Journal of Glaciology*, **57**(205), 917–928 (doi: 10.3189/002214311798043780)

Marsh OJ, Rack W, Golledge NR, Lawson W and Floricioiu D (2014) Grounding-zone ice thickness from InSAR: Inverse modelling of tidal elastic bending. *Journal of Glaciology*, **60**(221), 526–536 (doi: 10.3189/2014JoG13J033)

Morlighem M (2022) MEaSUREs BedMachine Antarctica, version 3 (doi: 10.5067/FPSU0V1MWUB6)

Morlighem M, Rignot E, Seroussi H, Larour E, Ben Dhia H and Aubry D (2011) A mass conservation approach for mapping glacier ice thickness. *Geophysical Research Letters*, **38**(19) (doi: https://doi.org/10.1029/2011GL048659)

Morlighem M, Rignot E, Mouginot J, Seroussi H and Larour E (2014) Deeply incised submarine glacial valleys beneath the Greenland ice sheet. *Nature Geoscience*, **7**(6), 418–422, ISSN 1752-0908 (doi: 10.1038/ngeo2167)

Morlighem M, Williams CN, Rignot E, An L, Arndt JE, Bamber JL, Catania G, Chauché N, Dowdeswell JA, Dorschel B, Fenty I, Hogan K, Howat I, Hubbard A, Jakobsson M, Jordan TM, Kjeldsen KK, Millan R, Mayer L, Mouginot J, Noël BPY, O'Cofaigh C, Palmer S, Rysgaard S, Seroussi H, Siegert MJ, Slabon P, Straneo F, van den Broeke MR, Weinrebe W, Wood M and Zinglersen KB (2017) BedMachine v3: Complete bed topography and ocean bathymetry mapping of greenland from multibeam echo sounding combined with mass conservation. *Geophysical Research Letters*, **44**(21), 11,051–11,061 (doi: https://doi.org/10.1002/2017GL074954)

Morlighem M and 36 others (2020) Deep glacial troughs and stabilizing ridges unveiled beneath the margins of the Antarctic ice sheet. *Nature Geoscience*, **13**, 132–137 (doi: 10.1038/s41561-019-0510-8)

Mottram R, Hansen N, Kittel C, van Wessem JM, Agosta C, Amory C, Boberg F, van de Berg WJ, Fettweis X, Gossart A, van Lipzig NPM, van Meijgaard E, Orr A, Phillips T, Webster S, Simonsen SB and Souverijns N (2021) What is the surface mass balance of Antarctica? An intercomparison of regional climate model estimates. *The Cryosphere*, **15**(8), 3751–3784 (doi: 10.5194/tc-15-3751-2021)

Mueller RD, Hattermann T, Howard SL and Padman L (2018) Tidal influences on a future evolution of the Filchner–Ronne Ice Shelf cavity in the Weddell Sea, Antarctica. *The Cryosphere*, **12**(2), 453–476 (doi: 10.5194/tc-12-453-2018)

Oerlemans J (1982) A model of the Antarctic Ice Sheet. *Nature*, **297**(5867), 550–553, ISSN 1476-4687 (doi: 10.1038/297550a0)

Padman L, Siegfried MR and Fricker HA (2018) Ocean tide influences on the Antarctic and Greenland ice sheets. *Reviews of Geophysics*, **56**, 142–184 (doi: 10.1002/2016RG000546)

Pattyn F (2017) Sea-level response to melting of Antarctic ice shelves on multi-centennial timescales with the fast Elementary Thermomechanical Ice Sheet model (f.ETISh v1.0). *Cryosphere*, **11**, 1851–1878 (doi: 10.5194/tc-11-1851-2017)

Pattyn F, Perichon L, Durand G, Favier L, Gagliardini O, Hindmarsh RC, Zwinger T, Albrecht T, Cornford S, Docquier D and et al (2013) Grounding-line migration in plan-view marine ice-sheet models: results of the ice2sea MISMIP3d intercomparison. *Journal of Glaciology*, **59**(215), 410–422 (doi: 10.3189/2013JoG12J129)

Robin G (1958) *Norwegian-British-Swedish Antarctic Expedition, 1949-52: Scientific Results. Vol. III : Seismic Shooting and Related Investigations*. Norsk Polarinstitutt

Rosier SH, Marsh OJ, Rack W, Gudmundsson GH, Wild CT and Ryan M (2017) On the interpretation of ice-shelf flexure measurements. *Journal of Glaciology*, **63**(241), 783–791 (doi: 10.1017/jog.2017.44)

Sayag R and Worster MG (2011) Elastic response of a grounded ice sheet coupled to a floating ice shelf. *Physical Review E - Statistical, Nonlinear, and Soft Matter Physics*, **84** (doi: 10.1103/PhysRevE.84.036111)

Sayag R and Worster MG (2013) Elastic dynamics and tidal migration of grounding lines modify subglacial lubrication and melting. *Geophysical Research Letters*, **40**(22), 5877–5881 (doi: 10.1002/2013GL057942)

Schoof C (2007) Ice sheet grounding line dynamics: Steady states, stability, and hysteresis. *Journal of Geophysical Research: Earth Surface*, **112**(F3) (doi: https://doi.org/10.1029/2006JF000664)

Schulson E and Duval P (2011) *Creep and Fracture of Ice*. Cambridge University Press (doi: 10.3189/S0022143000206254)

Seroussi H and 46 others (2020) ISMIP6 Antarctica: A multi-model ensemble of the Antarctic ice sheet evolution over the 21st century (doi: 10.5194/tc-14-3033-2020)

Seu R, Phillips RJ, Biccari D, Orosei R, Masdea A, Picardi G, Safaeinili A, Campbell BA, Plaut JJ, Marinangeli L, Smrekar SE and Nunes DC (2007) SHARAD sounding radar on the Mars Reconnaissance Orbiter. *Journal of Geophysical Research: Planets*, **112**(E5) (doi: https://doi.org/10.1029/2006JE002745)

Smith B and 14 others (2020) Pervasive ice sheet mass loss reflects competing ocean and atmosphere processes. *Science*, **368**(6496), 1239–1242 (doi: 10.1126/science.aaz5845)

Van Wessem JM and 18 others (2018) Modelling the climate and surface mass balance of polar ice sheets using RACMO2 - Part 2: Antarctica (1979-2016). *Cryosphere*, **12**, 1479–1498

Vaughan DG (1995) Tidal flexure at ice shelf margins. *Journal of Geophysical Research*, **100**, 6213–6224 (doi: 10.1029/94JB02467)

Warner RC and Budd WF (2000) Derivation of ice thickness and bedrock topography in data-gap regions over antarctica. *Annals of Glaciology*, **31**, 191–197 (doi: 10.3189/172756400781820011)